Modeling of DCIV Recombination Currents Using A Multistate Multiphonon Model

M. Bina*, Th. Aichinger†, G. Pobegen‡, W. Gös§, and T. Grasser§
*Christian Doppler Laboratory for Reliability in Microelectronics at the Institute for Microelectronics, TU Wien, Austria
†Penn State University, Department of Engineering Science and Mechanics, University Park, PA 16802, USA
‡KAI (Kompetenzzentrum für Automobil- und Industrieelektronik GmbH), Europastrasse 8, A-9524 Villach
§Institute for Microelectronics, TU Wien, Gusshausstrasse 27–29, Austria Email: bina@iue.tuwien.ac.at

***Abstract*—We study p-type metal-oxide-semiconductor field-effect transistors (pMOSFETs) using the direct-current-current-voltage (DCIV) method before and after bias temperature stress. The stress is varied over a wide range of temperatures using our polyheater technology. The ability of the SRH model and a multistate non-radiative multiphonon (NMP) model to meaningfully reproduce the acquired DCIV data is compared. It is demonstrated that the SRH model cannot capture the detailed features of the data and a more detailed model is required.**

I. Introduction

In recent years the interest in the Negative Bias Temperature Instability (NBTI) and stress-induced interface and oxide defects in MOS devices has rapidly increased [1]. Considerable effort has been invested to explain and understand the nature of defects generated in MOS devices during NBTI stress. First introduced by [2] and [3], the direct-current-current-voltage (DCIV) method is used to directly monitor the defect density by measuring the bulk current I_b, which is the result of the carrier recombination in the oxide and at the silicon-oxide interface (cf. Fig. 1). In order to extract any useable

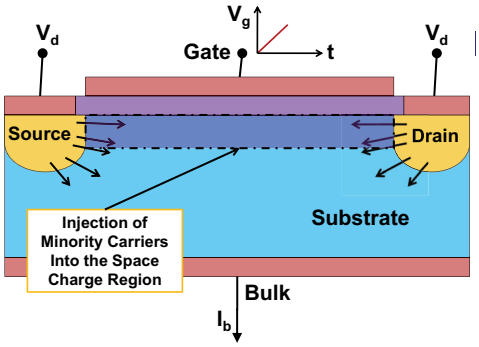

Fig. 1: During each DCIV experiment the device is swept from accumulation to inversion by changing the gate voltage, while the pn junctions are forward biased. This forward bias allows the injection of minority carriers into the space charge region, where they may recombine with a trap, causing a measurable bulk current.

defect densities from the measured bulk current a physically correct model is needed. To our best knowledge, so far all modeling attempts to describe DCIV experiments were based on the standard SRH theory [4], [5] for defects at the oxide-silicon interface or border traps. In these previous attempts structural relaxation of the lattice around the defect center [6], recently suggested to describe NBTI [7], was not considered. Furthermore it was pointed out by Reisinger *et al.* [8] that the trapping kinetics of oxide traps are temperature and strongly oxide field dependent. In this work we show using experimental DCIV data that structural relaxation cannot be neglected in the correct assessment of the recombination current when considering a wide range of bias temperature stress conditions.

II. Experimental Setup

For the measurement we used pMOSFETs with 30 nm thick $\mathrm{SiO_2}$ as gate dielectric. All pMOSFETs have been integrated with our polyheater technology [9] in order to be able to locally heat the devices up to 500°C. In order to monitor the stress induced degradation, DCIV experiments [2], [3] were performed on fresh devices before and after stress using a drain voltage V_d of 0.35 V to forward bias the pn junctions. For each stress temperature a fresh device was stressed for 10 seconds ($t_\mathrm{stress} = 10\,\mathrm{s}$) while applying a gate voltage of -20 V ($V_\mathrm{stress} = -20\,\mathrm{V}$ and $E_\mathrm{ox} \approx 6.7\,\mathrm{MV/cm}$). Directly after stress the devices were cooled down for $t_\mathrm{delay} = 200\,\mathrm{s}$ to room temperature at a gate voltage of -20 V (cf. Fig. 2). With the end of this cool down phase a DCIV curve for the now stressed device was recorded.

III. Models

The standard SRH model for interface traps and the recently introduced multistate NMP model for NBTI [11], [12] were used to describe the measurement data in order to compare their ability to reflect the NBTI stress dependent DCIV data. For the extraction all recombination centers, i.e. stress induced defects, were assumed to be at or near the silicon-oxide interface. The bulk current measured during the DCIV experiments is directly proportional to the number of recombination events [2], thus one can assume steady state conditions. Carrier recombination in the bulk, especially at the pn junctions, would cause a constant bulk current during the DCIV experiment. Since we did not observe a shift of the measured DCIV curves along the ordinate within the accuracy of the measurement equipment we can safely assume negligible carrier recombination in the bulk. Additionally geometrical effects were neglected, since large devices with a 30 nm thick gate dielectric and a nominal gate length larger

978-1-4577-0115-3/11/$26.00 ©2011 IEEE

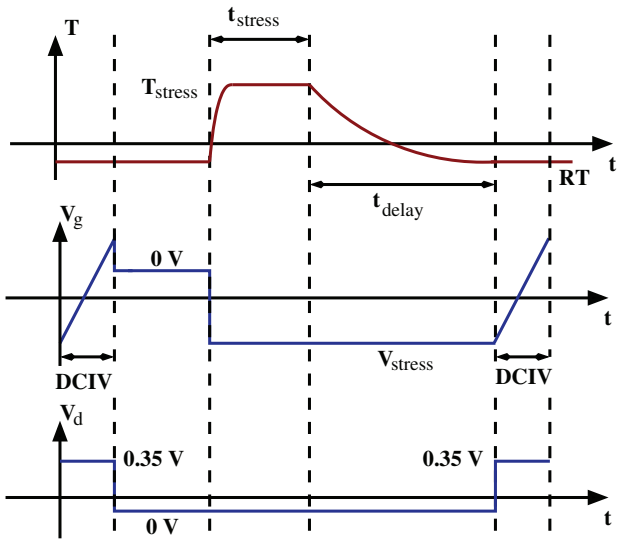

Fig. 2: Timeline of a single experiment. The upper part of the figure depicts the device temperature over time. The curve in the middle depicts the gate voltage over time. The bottom curve depicts the drain and source voltage over time. For each stress temperature T_{stress} a fresh device was used. Prior to stress an initial DCIV curve was recorded at room temperature. Afterwards the device was heated by integrated polyheaters almost instantly to the stress temperature T_{stress}, while a gate voltage $V_{\mathrm{g}} = V_{\mathrm{stress}}$ of -20 V was applied (bias temperature stress). Under these conditions the device was stressed for $t_{\mathrm{stress}} = 10\,\mathrm{s}$. With the end of the bias temperature stress phase the polyheaters are switched off and the device was cooled down for $t_{\mathrm{delay}} = 200\,\mathrm{s}$ to room temperature (RT), while the gate voltage was maintained at -20 V (V_{stress}). The gate voltage was kept at V_{stress} during cool down in order to minimize relaxation [10]. At the end of the cool down phase a DCIV experiment on the degraded device was performed at room temperature (cf. right side of the lower part of the figure).

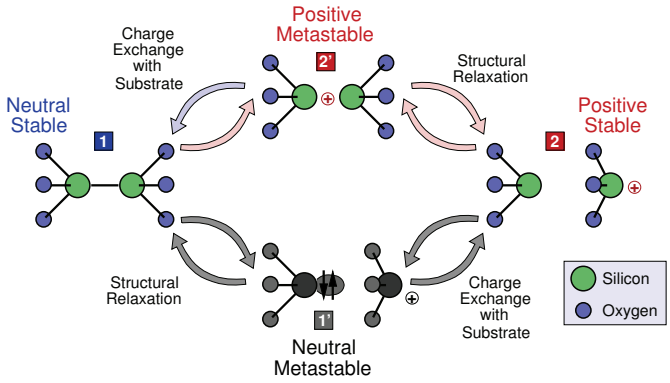

Fig. 3: The multistate NMP model from [11]. Depicted is the finite state diagram for a single oxide defect. State 1 is the stable and electrically neutral precursor state. Upon hole capture (red arrow from state 1 to state $2'$) the defect becomes positively charged and is meta-stable. A defect in state $2'$ can, upon the capture of an electron, undergo a transition back to the neutral and stable precursor state 1. The charge carrier exchange processes them self are modelled using NMP theory [13], [14]. Alternatively, a defect in state $2'$ can undergo the slow process of structural relaxation, becomes stable and stays positively charged (state 2). In state 2 the defect can either go back into state $2'$ or can capture an electron thus becoming electrically neutral and return to state $1'$. In state $1'$ the defect is neutral and can either by structural relaxation undergo a transition into the stable precursor state 1 or can capture a hole and thus change into the stable positively charged state 2. As a first approximation we neglected state $1'$ and transitions from and to this state (gray shaded).

than 100 nm were used. For the SRH model we used the formula originally derived in [5], which reads

$$R = \frac{0.5\sqrt{\sigma_{\mathrm{p}}\sigma_{\mathrm{n}}}n_{\mathrm{i}}\left(\exp\left(\beta\left(E_{\mathrm{fp}} - E_{\mathrm{fn}}\right)\right) - 1\right)}{\exp\left(\beta\left(E_{\mathrm{fp}} - E_{\mathrm{fn}}\right)/2\right)\cosh\left(\beta U_{\mathrm{S}}^{*}\right)\cosh\left(\beta U_{\mathrm{TI}}^{*}\right)}, \quad (1)$$

$$U_{\mathrm{S}}^{*} = \phi_{\mathrm{s}} + \ln\left(\sqrt{\sigma_{\mathrm{p}}\sigma_{\mathrm{n}}}\right) - \left(E_{\mathrm{fp}} + E_{\mathrm{fn}}\right)/2, \quad (2)$$

$$U_{\mathrm{TI}}^{*} = \left(E_{\mathrm{T}} - E_{\mathrm{i}}\right)\ln\left(\sqrt{\sigma_{\mathrm{p}}\sigma_{\mathrm{n}}}\right), \quad (3)$$

where n and p are the electron and hole carrier concentrations, n_{i} is the intrinsic carrier concentration, E_{fn} and E_{fp} are the quasi Fermi levels, E_{i} is the intrinsic energy, σ_{p} and σ_{n} are the constant hole and electron capture cross sections, ϕ_{s} is the surface potential, and $\beta = 1/k_{\mathrm{B}}T$.

In the following we make a few assumptions in order to simplify the multistate NMP model (cf Fig. 3). Since the DCIV method was used at room temperature to measure the post-stress recombination current, recovery of stress-induced defects during the DCIV measurement within the short experimental time window were assumed to be small. Additionally, we neglected state $1'$ in order to obtain a simplified approximation to the full multistate NMP model. In order to further simplify matters, we also assume that during each DCIV experiment only a negligible amount of traps anneal. These assumptions were experimentally justified by comparing DCIV curves for various measurement durations, i.e. different slopes of the gate voltage applied, whereas the measurements yielded the same DCIV curves. With the stated simplifications we derive a compact analytical version of the carrier recombination rate for the multistate NMP model. By defining effective rates we reduce the three remaining defect states (cf Fig. 3) to only two. The effective rates read [15],

$$k_{12} = \frac{k_{12'}k_{2'2}}{k_{2'1} + k_{2'2}} \quad \text{and} \quad k_{21} = \frac{k_{2'1}k_{22'}}{k_{2'1} + k_{2'2}}. \quad (4)$$

Employing Boltzmann statistics and applying our assumptions to the first order differential equations from [11] we obtain the following equation for the occupancy of a trap

$$\frac{df}{dt} = k_{21}(1 - f) - k_{12}f = 0, \quad (5)$$

Using the definition of the recombination rate for holes R_{p} in steady state

$$R = R_{\mathrm{p}} = R_{\mathrm{n}} = k_{12'}f - k_{2'1}(1 - f), \quad (6)$$

and inserting the solution of Equation (5), gives an analytical formula in the framework of a multistate NMP model for carrier recombination

$$R = -\frac{k_{22'}k_{2'2}\left(n_{\mathrm{i}}^{2} - np\right)\sigma_{\mathrm{p}}\sigma_{\mathrm{n}}v_{\mathrm{th}}^{\mathrm{n}}v_{\mathrm{th}}^{\mathrm{p}}}{N} \quad (7)$$

$$\begin{aligned} N = {} & \exp\left(\beta\epsilon_{12'}\right)k_{22'}n\sigma_{\mathrm{n}}v_{\mathrm{th}}^{\mathrm{n}} + \exp\left(\beta\epsilon_{2'1}\right)k_{2'2}p\sigma_{\mathrm{p}}v_{\mathrm{th}}^{\mathrm{p}} \\ & + \exp\left(\beta(-E_{\mathrm{i}} + \epsilon_{12'} + E_{\mathrm{T}} - \epsilon_{\mathrm{T}2'})\right)k_{2'2}n_{\mathrm{i}}\sigma_{\mathrm{n}}v_{\mathrm{th}}^{\mathrm{n}} \\ & + \exp\left(\beta(E_{\mathrm{i}} + \epsilon_{2'1} - E_{\mathrm{T}} - \epsilon_{\mathrm{T}2'})\right)k_{22'}n_{\mathrm{i}}\sigma_{\mathrm{p}}v_{\mathrm{th}}^{\mathrm{p}}, \end{aligned} \quad (8)$$

where $v_{\mathrm{th}}^{\mathrm{n}}$ and $v_{\mathrm{th}}^{\mathrm{p}}$ are the electron and hole carrier velocities, σ_{n} and σ_{p} are the constant electron and hole capture cross sections. For all simulations the constant capture cross sections σ_{n} and σ_{p} were fixed to a value of $2.0 \times 10^{-16}\,\mathrm{cm}^{2}$ for the SRH (1) and the multistate NMP model (7).

IV. Results

DCIV curves measured for various stress temperatures and normalized to the peak value for $T_{\mathrm{stress}} \approx 245°\mathrm{C}$ are shown in Fig. 4. The maximum value of the bulk current I_{b} increases with higher stress temperatures as expected. Also noteworthy is the broadening of the bell-shaped DCIV curve towards negative gate voltages, whereas there is almost no broadening towards positive gate voltages (cf Fig. 4 for $V_{\mathrm{g}} > -0.5\,\mathrm{V}$). This indicates that traps with higher activation energies are becoming active trapping centers at higher stress temperatures. A fit of the SRH model [4] for the post-stress measurement

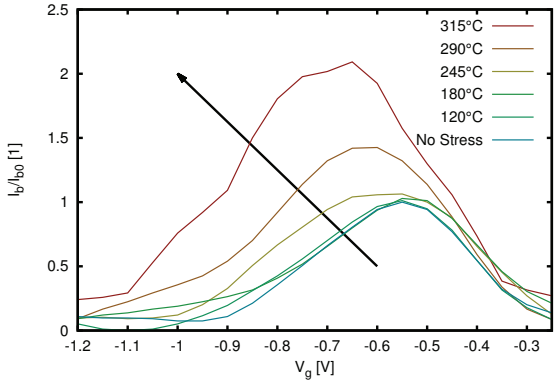

Fig. 4: For higher stress temperatures the peak in I_{b} is larger and the curve is broader towards negative gate voltages (black arrow), whereas the slope for gate voltages higher $-0.5\,\mathrm{V}$ remains nearly constant. Also noteworthy is the shoulder towards negative gate voltages for a stress temperature of $315°\mathrm{C}$.

data is shown in Fig. 5. It can be seen that the SRH model can reproduce the DCIV curve only for certain stress temperatures (in this case $T_{\mathrm{stress}} \approx 240°\mathrm{C}$), but not for a wide range of stress temperatures. Especially for stress temperatures above $315°\mathrm{C}$, when the DCIV bell-shaped curve develops a shoulder towards negative gate voltages, the SRH model cannot reproduce the experimental data as shown in Fig. 6. Noteworthy is the fact, as seen in Fig. 6, that the post-stress DCIV curve changes its shape for stress temperatures above

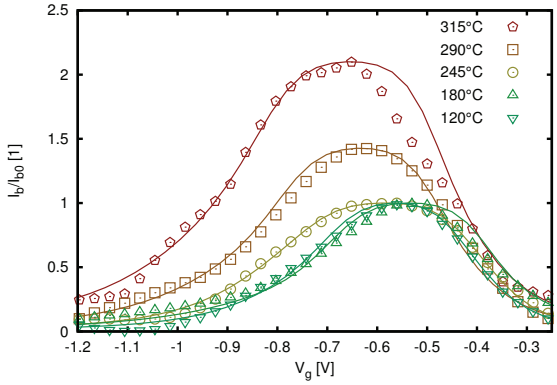

Fig. 5: Fits of the standard SRH model to the post-stress DCIV curves for various stress temperatures. Especially for higher stress temperatures, such as $315°\mathrm{C}$, the standard SRH model cannot reproduce the shape of the measurement data anymore.

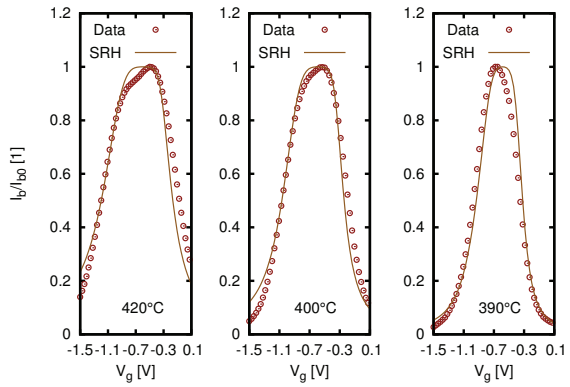

Fig. 6: Same as in Fig. 5 but for higher stress temperatures. At very high stress temperatures the post-stress DCIV curve develops a characteristic shoulder. The SRH model cannot predict any of the three DCIV curves, since it cannot reflect the characteristic shoulder.

$315\,°\mathrm{C}$. This explains why the SRH model, for which the recombination current exhibits a $\cosh^{-1}$ shape (cf. Equation (1)) for all temperatures [5], cannot reproduce the experimental data anymore. In contrast to the SRH model the multistate NMP model can give excellent fits to the data for all stress temperatures as shown in Fig. 7. This can be attributed to the fact that the multistate NMP model additionally considers structural relaxation (cf Fig. 3 and Fig. 10). To understand

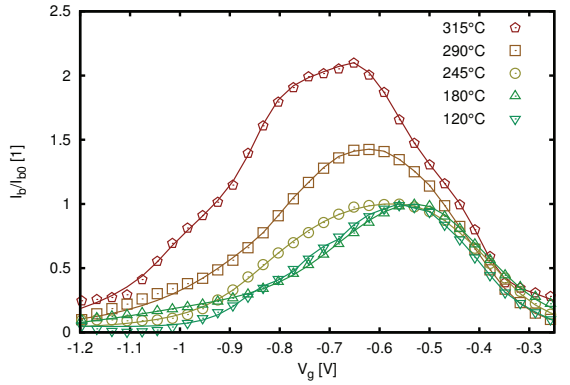

Fig. 7: In contrast to the fit for the SRH model (cf Fig. 5), the NMP model can explain the post-stress DCIV data for all stress temperatures used. Remarkable is the ability of the NMP model to reproduce the DCIV curve for a stress temperature of $315\,°\mathrm{C}$ with high accuracy.

why structural relaxation can explain the additional shoulder above a stress temperature of $315\,°\mathrm{C}$ in our data, we reformulated the carrier recombination terms in the multistate NMP model (7) and for the SRH model (2) such that both formulas have the same structure. The carrier recombination term for both models has the following structure

$$R = -\frac{\left(n_{\mathrm{i}}^2 - np\right)\sigma'_{\mathrm{p}}\sigma'_{\mathrm{n}}v_{\mathrm{th}}^{\mathrm{n}}v_{\mathrm{th}}^{\mathrm{p}}}{\tau'_{\mathrm{n}}(n+n_1)+\tau'_{\mathrm{p}}(p+p_1)}, \tag{9}$$

where τ'_{n} and τ'_{p} are the carrier lifetimes for electrons and holes and σ'_{n} and σ'_{p} are the capture cross sections for electrons and holes, respectively. These terms are model-dependent. For the

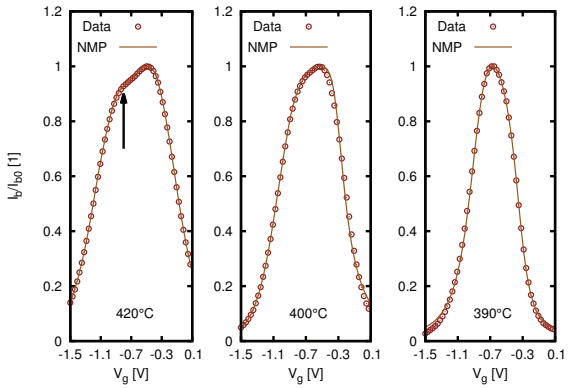

Fig. 8: For high stress temperatures it is possible to reproduce the post-stress DCIV data with good accuracy. Even the characteristic shoulder, best seen for $T_{\mathrm{stress}} = 420\,^{\circ}\mathrm{C}$, can be fitted with excellent accuracy.

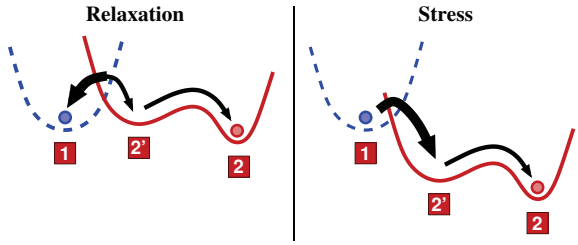

Fig. 9: A schematic representation of the adiabatic potentials used to define the transition rates (cf Fig. 3) for each defect. During relaxation of ΔV_{th} (low oxide field) the barrier for a trapped hole is low and the defect is very likely to emit this hole and undergo a transition from the charged state $2'$ to the neutral state 1 (left side). During stress (right side) the defect potential (dashed line) is raised due to the oxide field. Thus a defect is more likely to capture a hole and undergo a transition from the stable neutral state 1 to the charged meta-stable state $2'$ than vice versa (bold black arrow). While the capture and emission of charge carriers is strongly oxide field dependent, the transitions between state $2'$ and 2, describing the structural relaxation of the defect, depend on the energetic barriers $\epsilon_{22'}$, $\epsilon_{2'2}$ and temperature. This strong temperature dependence physically explains the temperature dependence of the effective charge capture cross sections.

SRH model the capture cross sections have fixed values, where

$$\sigma'_{\mathrm{n}} = \sigma_{\mathrm{n}} = 2.0 \times 10^{-16}\,\mathrm{cm}^2, \tag{10}$$

$$\sigma'_{\mathrm{p}} = \sigma_{\mathrm{p}} = 2.0 \times 10^{-16}\,\mathrm{cm}^2. \tag{11}$$

In contrast, the multistate NMP model gives

$$\sigma'_{\mathrm{n}} = \frac{\exp\left(\beta\epsilon_{2'1}\right)}{k_{22'}k_{2'2}}\sigma_{\mathrm{n}} = \frac{\exp\left(\beta\epsilon_{2'1}\right)}{\nu^2\exp\left(-\beta\epsilon_{22'}\epsilon_{2'2}\right)}\sigma_{\mathrm{n}} \tag{12}$$

and

$$\sigma'_{\mathrm{p}} = \frac{\exp\left(\beta\epsilon_{12'}\right)}{k_{22'}k_{2'2}}\sigma_{\mathrm{p}} = \frac{\exp\left(\beta\epsilon_{12'}\right)}{\nu^2\exp\left(-\beta\epsilon_{22'}\epsilon_{2'2}\right)}\sigma_{\mathrm{p}}. \tag{13}$$

Furthermore, the carrier lifetimes differ strongly between the SRH model and the multistate NMP model [11]. Thus it can be stated that the effective capture cross sections of the multistate NMP model are device temperature, oxide field and parameter dependent, while those of the SRH model are always constant. By adjusting the energetic barriers ($\epsilon_{22'}$ and $\epsilon_{2'2}$) describing the structural relaxation (cf Fig. 9 and Fig. 3) it is possible to even perfectly fit the DCIV curves measured after high temperature stress (cf Fig. 8). Fig. 10 depicts how the shoulder, which the DCIV curves exhibits for stress temperatures above $315\,^{\circ}\mathrm{C}$, can be described using a multistate NMP model. If structural relaxation is neglected (cf state 2 in Fig. 3) one obtains a standard NMP model [13], [14]. For the standard NMP model the energetic barriers ($\epsilon_{22'}$ and $\epsilon_{2'2}$) describing the structural relaxation are zero. Thus the effective capture cross sections of the standard NMP model reduce to

$$\sigma'_{\mathrm{n}} = \frac{\exp\left(\beta\epsilon_{2'1}\right)}{\underbrace{k_{22'}}_{1}\underbrace{k_{2'2}}_{1}}\sigma_{\mathrm{n}} = \exp\left(\beta\epsilon_{2'1}\right)\sigma_{\mathrm{n}} \tag{14}$$

and

$$\sigma'_{\mathrm{p}} = \frac{\exp\left(\beta\epsilon_{12'}\right)}{\underbrace{k_{22'}}_{1}\underbrace{k_{2'2}}_{1}}\sigma_{\mathrm{p}} = \exp\left(\beta\epsilon_{12'}\right)\sigma_{\mathrm{p}}. \tag{15}$$

This reduction of the multistate NMP model results in the loss of its strong temperature dependence [12] and in the loss of two degrees of freedom for parameter extraction.

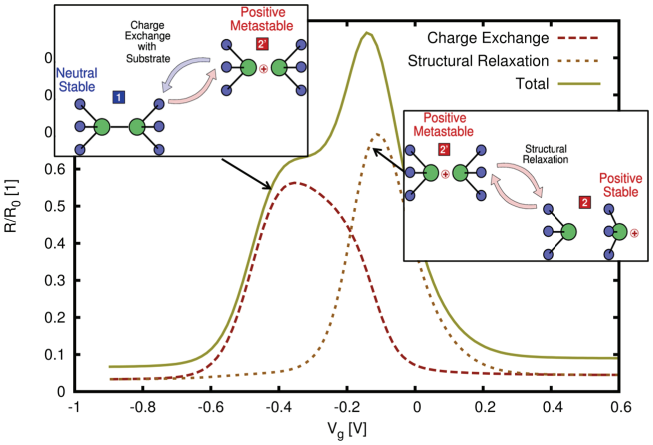

Fig. 10: When the exchange of charge carriers with the substrate dominates the recombination current exhibits a bell-shaped curve towards negative gate voltages. Whereas when structural relaxation dominates the recombination current exhibits a bell-shaped curve towards positive gate voltages. The weighted sum of these two theoretical recombination currents gives a bell shaped curve with an additional shoulder.

V. Summary

We have investigated the capability of the SRH and NMP model to explain DCIV measurements for pMOS devices after NBTI stress at various stress temperatures. The results clearly show the importance of structural relaxation for a proper description of recombination currents in a pMOS after NBTI stress. We have successfully shown that a multistate NMP model can explain DCIV measurement data for various stress temperatures. No such agreement could be obtained with the conventional SRH model. As such, the data obtained from DCIV measurements is consistent with NBTI stress and recovery data, which can also only be described using an NMP model [11], [16].

References

[1] T. Grasser, B. Kaczer, W. Gös, H. Reisinger, T. Aichinger, P. Hehenberger, P.-J. Wagner, F. Schanovsky, J. Franco, P. Roussel, and M. Nelhiebel, "Recent Advances in Understanding the Bias Temperature Instability," in *IEDM*, Dec. 2010, pp. 82–85.

[2] C. Sah, "Effects of Surface Recombination and Channel on p-n Junction and Transistor Charactersitics," *T-ED*, vol. 9, pp. 94–108, 1962.

[3] A. Neugroschel, C.-T. Sah, K. Han, M. Carroll, T. Nishida, J. Kavalieros, and Y. Lu, "Direct-Current Measurements of Oxide and Interface Traps on Oxidized Silicon," *T-ED*, vol. 42, no. 9, pp. 1657–1662, 1995.

[4] W. Shockley and W. Read, "Statistics of the Recombinations of Holes and Electrons," *PR*, vol. 87, no. 5, pp. 835–842, 1952.

[5] J. Cai and C.-T. Sah, "Interfacial Electronic Traps in Surface Controlled Transistors," *T-ED*, vol. 47, no. 3, pp. 576 –583, mar 2000.

[6] J. Conley, P. Lenahan, A. Lelis, and T. Oldham, "Electron Spin Resonance Evidence for the Structure of a Switching Oxide Trap: Long Term Structural Change at Silicon Dangling Bond Sites in SiO_2 ," *APL*, vol. 67, no. 15, pp. 2179–2181, 1995.

[7] T. Grasser, T. Aichinger, G. Pobegen, H. Reisinger, P.-J. Wagner, J. Franco, M. Nelhiebel, and B. Kaczer, "The 'Permanent' Component of NBTI: Composition and Annealing," in *IRPS*, Apr. 2011, pp. 605–613.

[8] H. Reisinger, T. Grasser, W. Gustin, and C. Schlünder, "The Statistical Analysis of Individual Defects Constituting NBTI and its Implications for Modeling DC- and AC-Stress," in *IRPS*, May 2010, pp. 7–15.

[9] T. Aichinger, M. Nelhiebel, S. Einspieler, and T. Grasser, "*In Situ* Polyheater – A Reliable Tool for Performing Fast and Defined Temperature Switches on Chip," *T-DMR*, vol. 10, no. 1, pp. 3–8, 2010.

[10] T. Grasser, T. Aichinger, H. Reisinger, J. Franco, P.-J. Wagner, M. Nelhiebel, C. Ortolland, and B. Kaczer, "On the 'Permanent' Component of NBTI," in *IIRW*, Oct. 2010.

[11] T. Grasser, H. Reisinger, P.-J. Wagner, W. Goes, F. Schanovsky, and B. Kaczer, "The Time Dependent Defect Spectroscopy (TDDS) for the Characterization of the Bias Temperature Instability," in *IRPS*, May 2010, pp. 16–25.

[12] T. Grasser, "Stochastic Charge Trapping in Oxides: From Random Telegraph Noise to Bias Temperature Instabilities," *Microelectronics Reliability*, 2011.

[13] D. Lang and C. Henry, "Nonradiative Recombination at Deep Levels in GaAs and GaP by Lattice-Relaxation Multiphonon Emission," *PRL*, vol. 35, no. 22, pp. 1525–1528, 1975.

[14] F. Schanovsky, W. Gös, and T. Grasser, "Multiphonon Hole Trapping from First Principles," *JVST B*, vol. 29, no. 1, pp. 01A2011–01A2015, 2011.

[15] T. Grasser, H. Reisinger, W. Gös, T. Aichinger, P. Hehenberger, P. Wagner, M. Nelhiebel, J. Franco, and B. Kaczer, "Switching Oxide Traps as the Missing Link between Negative Bias Temperature Instability and Random Telegraph Noise," in *IEDM*, 2009, pp. 729–732.

[16] T. Grasser, B. Kaczer, W. Gös, T. Aichinger, P. Hehenberger, and M. Nelhiebel, "A Two-Stage Model for Negative Bias Temperature Instability," in *IRPS*, 2009, pp. 33–44.

Questions and Answers

Q1: You mentioned that the traps are located close to the interface in your simulations. Is this trap still an E' center (oxide trap) or could it also be a Pb center? How would this affect the effective capture cross section in the latter case?

A1: The trap in the multi-state NMP model is only characterized by certain properties, such as energies of the equilibrium configurations, the transition barriers, and trap depth. Each defect having these properties is a possible candidate in this model, which includes E' and Pb centers. Given the current lack of experimental and theoretical details regarding these parameters, the defect type does not necessarily affect the effective capture cross section.

Q2: Why did you anticipate that an E' center rather than the Pb center is the dominating trap in your model?

A2: The model was set up using an E' center as an example, which shows a number of interesting properties observed in detailed ESR studies. Still, the model only uses the adiabatic defect potentials and is therefore rather general. In particular, we do not imply that we assume the E' center to be the dominating trap type.

Q3: Are the physics different at 400°C than at say room temperature?

A3: We are not aware of any changes in the defect properties for temperatures from room temperature up to 400°C for the devices used in this study.

Q4: Could NBTI be predicted accurately at 400°C?

A4: For the post-stress DCIV measurements used in our study this seems to be the case.